Available online at www.sciencedirect.com

SciVerse ScienceDirect

Procedia Engineering 00 (2013) 000–000

Procedia Engineering

www.elsevier.com/locate/procedia

12th International Conference on Computing and Control for the Water Industry, CCWI2013

Integrated mathematical model of a MBR reactor including biopolymer kinetics and membrane fouling

Tomasz Janus[a,*]

[a]*De Montfort University, The Gateway, LE1 9BH Leicester, United Kingdom*

Abstract

This paper briefly describes an integrated mathematical model of an immersed membrane bioreactor (MBR) with hollow fibre outside-in membranes. The integrated model is composed of three interconnected submodels: the activated sludge model (ASM) extended with soluble and bound biopolymer kinetics, the membrane fouling model, and the interface model relating cake back-transport rate to air-scour intensity and specific cake resistance to concentration of extracellular polymeric substances (EPS). The integrated model is simulated on the plant layout used in the BSM-MBR benchmark model of Maere et al. (2011) and predicts similar effluent quality to BSM-MBR whilst additionally enabling predictions of the transmembrane pressure (TMP) and of the effects of various operating conditions on membrane fouling.

Selection and peer-review under responsibility of the CCWI2013 Committee.

Keywords: Activated Sludge, Biopolymers, Integrated model, Membrane bioreactor, MBR, EPS, SMP, Simulation, Wastewater treatment

1. Introduction

MBR-based solutions are becoming more wide-spread in municipal as well as industrial wastewater treatment. What the technology is missing at the moment however is general-purpose mathematical models. Such models would allow to carry out similar simulation-based studies on MBR systems to what is already possible for other wastewater treatment processes such as, e.g. conventional activated sludge plants (CASPs). Until now only a handful of such MBR models have been developed and described in scientific literature although recent years have seen some important developments in the area of MBR modelling. Despite of these developments most models provide rather simplistic description of, either activated sludge kinetics, membrane fouling, or both. They are also unable to represent the main synergistic interactions that occur between various parts of a MBR such as, e.g. links between EPS and SMP kinetics and membrane fouling. Some of such models are briefly described below.

Zarragoitia-González et al. (2008) linked the activated sludge model of Lu et al. (2001) with a comprehensive membrane fouling model of Li and Wang (2006). Di Bella et al. (2008) linked an ASM1-based SMP kinetic model with membrane fouling equations based on the model of Lee et al. (2002). Unfortunately in their paper, links between SMP and irreversible fouling have not been modelled. Additionally, in both publications, Petersen matrices of the biological models do not pass a mass-balance check.

* Tomasz Janus. Tel.: +44-116-257-7070
E-mail address: tjanus@dmu.ac.uk

Selection and peer-review under responsibility of the CCWI2013 Committee.

Nomenclature

a	fraction of SMP contributing to irreversible fouling (–)
b	flux dependency coefficient in the irreversible fouling equation (L^{-1} m^2 h)
$d_{f,o}$	outer fibre diameter (m)
d_{slug}	diameter of the Taylor bubble (m)
f_{BAP}	fraction of S_{BAP} produced during biomass decay (gCOD $gCOD^{-1}$)
$f_{EPS,da}$	fraction of X_{EPS} produced during autotrophic biomass decay (gCOD $gCOD^{-1}$)
$f_{EPS,dh}$	fraction of X_{EPS} produced during heterotrophic biomass decay (gCOD $gCOD^{-1}$)
$f_{EPS,a}$	fraction of X_{EPS} produced during autotrophic biomass growth (gCOD $gCOD^{-1}$)
$f_{EPS,h}$	fraction of X_{EPS} produced during heterotrophic biomass growth (gCOD $gCOD^{-1}$)
f_M	S_{UAP} and S_{BAP} retention on the membrane (–)
f_S	fraction of S_S produced during X_{EPS} hydrolysis (gCOD $gCOD^{-1}$)
i_{XBAP}	nitrogen (N) content of S_{BAP} (gN $gCOD^{-1}$)
i_{XEPS}	nitrogen (N) content of X_{EPS} (gN $gCOD^{-1}$)
k_i	irreversible fouling strength (m kg^{-1})
$k_{h,EPS,20}$	maximum X_{EPS} hydrolysis rate at 20°C (d^{-1})
k_r	irreversible fouling strength (kg m^{-2} s^{-1})
K_{BAP}	half-saturation constant for S_{BAP} (gCOD m^{-3})
K_{UAP}	half-saturation constant for S_{UAP} (gCOD m^{-3})
l_f	distance between two fibres (m)
$\dot{m}_{r,back}$	mass flux of solids detaching from the cake and the membrane (kg m^{-2} s^{-1})
n	cake compressibility factor (–)
J	permeate flux (L m^{-2} h^{-1})
R_i	resistance due to irreversible fouling (m^{-1})
R_m	clean membrane resistance (m^{-1})
R_r	resistance due to reversible fouling (m^{-1})
R_t	total membrane resistance (m^{-1})
S_{BAP}	concentration of biomass associated products (BAP) (gCOD m^{-3})
S_{UAP}	concentration of utilisation associated products (UAP) (gCOD m^{-3})
t_f	filtration cycle duration time (s)
T_l	liquid temperature (°C)
v_{sg}	superficial gas velocity (cm s^{-1})
v_{sl}	superficial liquid velocity (cm s^{-1})
X_{EPS}	concentration of extracellular polymeric substances (EPS) (gCOD m^{-3})
X_{MLSS}	concentration of mixed liquor suspended solids (MLSS) (g m^{-3})
Y_{SMP}	yield coefficient for heterotrophic growth on S_{UAP} and S_{BAP} (gCOD $gCOD^{-1}$)
α	oxygen transfer coefficient (–)
α_c	specific cake resistance under field conditions (m kg^{-1})
$\alpha_{c,0}$	specific cake resistance at atmospheric pressure (m kg^{-1})
γ_A	fraction of S_{UAP} produced during autotrophic growth (gCOD $gCOD^{-1}$)
γ_H	fraction of S_{UAP} produced during heterotrophic growth (gCOD $gCOD^{-1}$)
γ_m	empirically determined proportionality coefficient in the cake detachment equation (Pa^{-1} s^{-1})
ΔP	trans-membrane pressure (Pa)
ΔP_{crit}	threshold pressure below which no cake compression occurs (Pa)
η_b	fraction of cake resistance which cannot be removed through backwashing (–)
λ_m	static friction coefficient in the cake detachment equation (–)
μ	dynamic water viscosity (Pa·s)
$\mu_{BAP,20}$	maximum specific heterotrophic growth rate on S_{BAP} at 20°C (d^{-1})
$\mu_{UAP,20}$	maximum specific heterotrophic growth rate on S_{UAP} at 20°C (d^{-1})
τ	filtration time (s)
τ_w	shear stresses acting on the cake as a results of air flow (Pa)

Mannina et al. (2011) improved the model of Di Bella et al. (2008) by swapping the non-mass and charge conserving model of Lu et al. (2001) with a modified ASM1 model implementing the SMP kinetics proposed by Jiang et al. (2008). The filtration model was modified to include more fouling mechanisms whilst keeping the sectional model approach of Lee et al. (2002) and the deep bed filtration equations introduced originally in Di Bella et al. (2008). Although their model was found to be in good agreement with the measurements collected on a MBR pilot plant, it suffers from the same weakness as the model of Di Bella et al. (2008), i.e. irreversible fouling is not related to SMP concentration in the bulk liquid. Most recently Suh et al. (2013) developed an integrated MBR model based on the benchmark simulation layout of Maere et al. (2011), combined EPS and SMP production ASM3-based model (CES-ASM3) of Janus and Ulanicki (2010) and the membrane fouling model of Li and Wang (2006). Their model again suffers from the same limitation as the previously outlined integrated models due to the fact that irreversible fouling has not been linked to SMP.

The integrated MBR model developed in this study differs from the models mentioned in the previous paragraph in several aspects. First, the biological model predicts the concentrations of both soluble (SMP) as well as bound (EPS) polymers whilst maintaining the structure of the ASM1 model, hence allowing easy comparison of the results with BSM1 and BSM-MBR benchmark models. Second, the fouling model has a simple structure and a small number of parameters which are easily identifiable with a 'pen and ruler' approach using flux and pressure data from flux stepping experiments. Third, both the reversible and the irreversible fouling is in a functional relationship with biopolymer concentrations in the bulk liquid. Whilst irreversible fouling is assumed to be caused by SMP, reversible fouling is accelerated by the presence of EPS which lead to an increase in the specific cake resistance α_c. Fourth, cake detachment depends on air-scouring rate accordingly to the shear stress vs. superficial gas velocity relationship obtained from the steady-state slug flow model of Zaisha and Dukler (1993).

2. Aims and Objectives

The main aim of this study is to create a mathematical model of an immersed MBR reactor which will allow to carry out simulation-based process designs, process and energy optimisation studies and model-based control strategy designs for MBR systems in a similar way to what is currently possible for conventional treatment processes. Such model will also enable integration of MBR process simulation within larger projects such as simulation of whole wastewater treatment plants (WWTPs) or integrated catchment modelling (ICM) studies. The main objective of an integrated simulation of MBR reactors is to improve the designs of the existing MBR systems in terms of energy-efficiency, resilience and effluent quality.

3. Activated Sludge Model with SMP and EPS kinetics

The biological model used in this study, later referred to as CES-ASM1 (combined EPS and SMP ASM1-based model) incorporates the unified theory of production and degradation of SMP and EPS developed by Laspidou and Rittmann (2002) within ASM1, although with one significant conceptual correction. Whilst Laspidou and Rittmann (2002) assume that the biomass associated products (BAP) in the system originate from the hydrolysis of EPS, researchers such as Aquino and Stuckey (2008) postulate that BAP is produced during EPS hydrolysis as well as during bacterial cell decay. In fact, BAP had already been defined by Lu et al. (2001) as the SMP fraction strictly originating from biomass decay. The lack of direct active cell decay-related SMP production in Laspidou and Rittmann (2002) was found to be the main cause of discrepancies between the model predictions and the measurements with regards to SMP (Menniti and Morgenroth, 2010). CES-ASM hence provides the mechanisms for BAP production due to both EPS hydrolysis and biomass decay. The metabolic pathways of SMP and EPS in the biological model are visualised in Fig. 1. CES-ASM1 was calibrated on the experimental data obtained from a batch and a continuous-flow lab scale bioreactor and a full-scale continuous-flow bioreactor as described in Janus and Ulanicki (2010). Results of the CES-ASM1 calibration study can be found alongside the calibration results of CES-ASM3 in Janus and Ulanicki (2010). Process rate expressions for the SMP and EPS kinetics are shown in Table 1 whilst Table 2 presents the Petersen matrix and the composition matrix. All other process rates in the model are the same as in ASM1 from the publication of Henze et al. (2000).

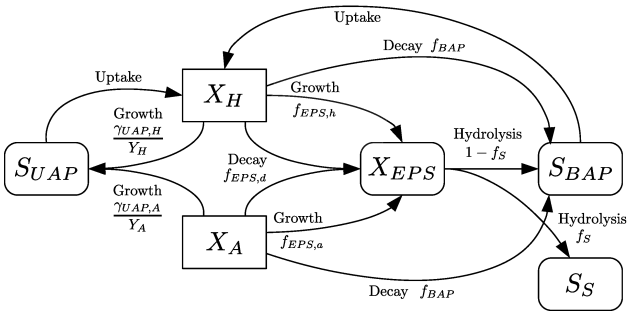

Fig. 1. EPS and SMP formation and utilisation pathways in the biological model.

Table 1. Process rate expressions for the SMP and EPS kinetics in the biological model.

Symbol	Process	Process rate equation
$p_{1,b}$	Aerobic growth on S_{BAP}	$e^{-0.069\,(20-T_l)}\ \mu_{BAP,20}\ \frac{S_{BAP}}{K_{BAP}+S_{BAP}}\ \frac{S_O}{K_{OH}+S_O}\ \frac{S_{ALK}}{K_{ALKH}+S_{ALK}}\ X_H$
$p_{1,c}$	Aerobic growth on S_{UAP}	$e^{-0.069\,(20-T_l)}\ \mu_{UAP,20}\ \frac{S_{UAP}}{K_{UAP}+S_{UAP}}\ \frac{S_O}{K_{OH}+S_O}\ \frac{S_{ALK}}{K_{ALKH}+S_{ALK}}\ X_H$
$p_{2,b}$	Anoxic growth on S_{BAP}	$e^{-0.069\,(20-T_l)}\ \mu_{BAP,20}\ \eta_g\ \frac{S_{BAP}}{K_{BAP}+S_{BAP}}\ \frac{K_{OH}}{K_{OH}+S_O}\ \frac{S_{NO}}{K_{NO}+S_{NO}}\ \frac{S_{ALK}}{K_{ALKH}+S_{ALK}}\ X_H$
$p_{2,c}$	Anoxic growth on S_{UAP}	$e^{-0.069\,(20-T_l)}\ \mu_{UAP,20}\ \eta_g\ \frac{S_{UAP}}{K_{UAP}+S_{UAP}}\ \frac{K_{OH}}{K_{OH}+S_O}\ \frac{S_{NO}}{K_{NO}+S_{NO}}\ \frac{S_{ALK}}{K_{ALKH}+S_{ALK}}\ X_H$
p_7	Hydrolysis of X_{EPS}	$e^{-0.11\,(20-T_l)}\ k_{h,EPS,20}\ X_{EPS}$

4. Membrane fouling model

The membrane fouling model is based on the concept of Liang et al. (2006) where fouling is divided into short-term reversible fouling and long-term irreversible fouling, graphically represented in Fig. 2a. Both processes are described with two first order ordinary differential equations (ODEs) which describe an increase in the membrane resistance due to, respectively, irreversible fouling (Eq. 1) and reversible fouling (Eq. 2). The model additionally accounts for cake compressibility (Eq. 7), cake detachment due to presence of airflow/crossflow (Eq. 5), backwashing (Eq. 6), and flux-dependent soluble microbial products (SMP) deposition. Equation relating the fraction of SMP leading to irreversible fouling to the permeate flux follows the model proposed by Ye et al. (2006) who found, through experimental analysis, that the fraction of alginate proteins depositing inside the membrane pores is in an exponential relationship with flux. The cake detachment model uses Equation 5 proposed by Nagaoka et al. (1998) in which cake detachment rate is proportional to the shear stress on the membrane wall τ_w and is diminished by a pressure dependent static friction term $\lambda_m \Delta P$ which determines the combined effects of cake consistency and attachment to membrane surface. Backwashing is assumed to be an instantaneous process in which reversible resistance at the beginning of the $(j+1)^{\text{th}}$ filtration cycle is equal to the fraction of reversible resistance at the end of the previous j^{th} filtration cycle - see Eq 6. We assumed that $\eta_b = 0$, i.e. all reversible fouling is removed in a single backwash.

$$\dot{R}_i = a\, k_i\, \mathrm{e}^{b\,J}\, J\ (S_{UAP} + S_{BAP}) \tag{1}$$

$$\dot{R}_r = \alpha_c\, (J\, X_{MLSS} - \dot{m}_{r,back}) \tag{2}$$

$$R_t = R_m + R_i + R_r \tag{3}$$

$$\Delta P = J/\left[\mu\ (R_m + R_i + R_r)\right] \tag{4}$$

$$\dot{m}_{r,back} = k_r\, (\tau_w - \lambda_m\, \Delta P) \tag{5}$$

$$\forall\, j \in \mathbb{N}\ :\ R_r^{j+1}(\tau = 0) = \eta_b\, R_r^{j}\,(\tau = t_f) \tag{6}$$

$$\alpha_c = \alpha_{c,0}\ (\Delta P/\Delta P_{crit})^n \tag{7}$$

Table 2. Stoichiometric (Petersen) and composition matrix for the biological model, j: process, i: component.

	Model components i	1	2	3	4	5	6	7	8	9	10	11	12	13	14	15	16	17
j	Processes	S_I	S_S	X_I	X_S	X_H	X_{EPS}	S_{UAP}	S_{BAP}	X_A	X_P	S_O	S_{NO}	S_{N_2}	S_{NH}	S_{ND}	X_{ND}	S_{ALK}
	Heterotrophic organisms																	
p_1	Ammonification														1	−1		$\frac{1}{14}$
p_{2a}	Aer. growth on S_S		$-\frac{1}{Y_H}$			1	$-f_{EPS,h}$	$\frac{\gamma_H}{Y_H}$				x_{2a}			y_{2a}			$-\frac{i_{XB}}{14}$
p_{2b}	Aer. growth on S_{BAP}					1	$-f_{EPS,h}$		$-\frac{1}{Y_{SMP}}$			x_{2b}			y_{2b}			$-\frac{i_{XB}}{14}$
p_{2c}	Aer. growth on S_{UAP}					1	$-f_{EPS,h}$	$-\frac{1}{Y_{SMP}}$				x_{2c}			y_{2c}			$-\frac{i_{XB}}{14}$
p_{3a}	Anox. growth on S_S		$-\frac{1}{Y_H}$			1	$-f_{EPS,h}$	$\frac{\gamma_H}{Y_H}$					x_{3a}	$-x_{3a}$	y_{3a}			$\frac{1-Y_H}{40\,Y_H}-\frac{i_{XB}}{14}$
p_{3b}	Anox. growth on S_{BAP}					1	$-f_{EPS,h}$		$-\frac{1}{Y_{SMP}}$				x_{3b}	$-x_{3b}$	y_{3b}			$\frac{1-Y_H}{40\,Y_H}-\frac{i_{XB}}{14}$
p_{3c}	Anox. growth on S_{UAP}					1	$-f_{EPS,h}$	$-\frac{1}{Y_{SMP}}$					x_{3c}	$-x_{3c}$	y_{3c}			$\frac{1-Y_H}{40\,Y_H}-\frac{i_{XB}}{14}$
p_4	Decay of heterotrophs				$1-f_P-f_{EPS,dh}-f_{BAP}$	−1	$f_{EPS,dh}$		f_{BAP}		f_P						$i_{XP}-f_P\,i_{XP}$	
p_5	Hydrolysis of org. compounds		1		−1													
p_6	Hydrolysis of org. N															1	−1	
p_7	Hydrolysis of X_{EPS}		f_S				−1	$1-f_S$								$i_{XEPS}-i_{XBAP}\,(1-f_S)$		
	Autotrophic organisms																	
p_8	Aerobic growth of autotrophs						$f_{EPS,a}$	$\frac{\gamma_A}{Y_A}$		$1-f_{EPS,a}$		$-\frac{\frac{64}{14}-Y_A}{Y_A}$	$\frac{1}{Y_A}$		$-i_{XB}-\frac{1}{Y_A}$			$-\frac{i_{XB}}{14}-\frac{1}{7\,Y_A}$
p_9	Decay of autotrophs				$1-f_P-f_{EPS,da}-f_{BAP}$		$f_{EPS,da}$		f_{BAP}	−1	f_P						$i_{XP}-f_P\,i_{XP}$	
	Composition matrix																	
1	ThOD (g ThOD)	1	1	1	1	1	1	1	1	1	1	-1	$-\frac{64}{14}$	$-\frac{24}{14}$				
2	Nitrogen (g N)					i_{XB}	i_{XEPS}		i_{XBAP}	i_{XB}	i_{XP}		1	1	1	1	1	
3	Ionic charge (Mole$^+$)												$-\frac{1}{14}$		$\frac{1}{14}$			-1

This model assumes that ThOD is identical to the measured COD. 1 gS_O = -1 gThOD, 1 gS_{NH} = 0 gThOD, 1gS_{NO} = -64/14 gThOD, 1 gS_{N_2} = -24/14 gThOD.

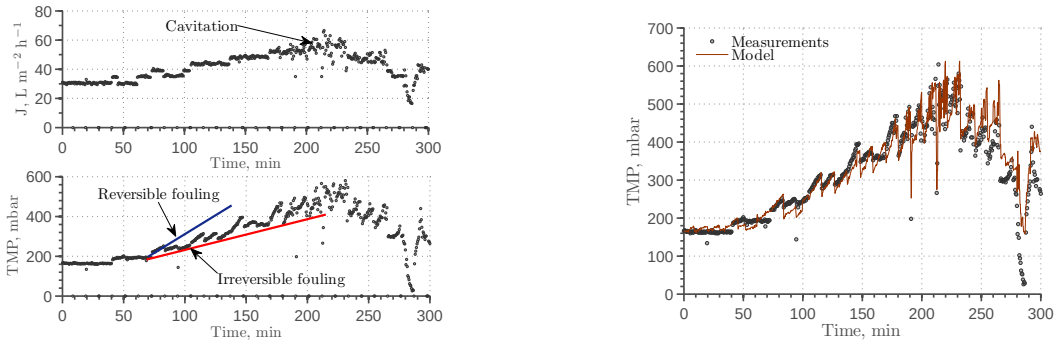

Fig. 2. (a) Representation of reversible and irreversible fouling (b) results of model calibration on data from a short-term flux-stepping experiment.

The model was calibrated on the data obtained in a short-term flux stepping experiment and during long-term operation of a pilot-scale membrane bioreactor (MBR), and exhibits good accuracy for its designated application and within the intended operating range. The calibration results are described in more detail in Janus et al. (2009) although the model used in this study uses a different equation for SMP deposition vs. flux, as mentioned above.

5. Air scouring

The relationship between shear stresses on the membrane surface τ_w and superficial gas velocity v_{sg}, hence the airflow rate, has been obtained through simulation of a slug-flow problem with a steady-state model of Zaisha and Dukler (1993) and a geometric model of a hollow-fibre module adopted from Busch et al. (2007). The geometric model assumes that all fibres are staggered, such that three neighbouring fibres form an equilateral triangle. The model assumes that slug-flow is fully developed, axially symmetric, isothermal, steady-state, and under low pressure conditions. Both phases are at an equilibrium, i.e. no one-directional mass transfer occurs between the phases whilst coalescence and breakage happen at equal rates. It is also assumed that the flow geometry does not change in time, i.e. the hollow-fibre membrane bundles do not sway due to velocity and pressure gradients developing in the bulk liquid. v_{sl} is related to v_{sg} using a modified Chisti equation as proposed by Böhm et al. (2012). The slug-flow model was simulated with MATLAB's Optimization Toolbox function `lsqnonlin` for a range of superficial gas velocities between 1 and 5 m s^{-1} which satisfy the aeration demands per membrane area (SADm) of 0.20-1.0 m^3 m^{-2} h^{-1}. The average shear stresses τ_w on the fibre surface were calculated for different values of v_{sg}, T_l and X_{TSS}. It was found that τ_w can be approximated with a third-order polynomial with respect to v_{sg} given in Eq. 8 where each coefficient p_i is in a functional relationship with X_{TSS} and T_l accordingly to Eq. 9.

$$\tau_w(v_{sg}) = p_1\,(v_{sg})^3 + p_2\,(v_{sg})^2 + p_3\,(v_{sg}) + p_4 \tag{8}$$

$$p_i = a_1 + a_2\,X_{TSS} + a_3\,T_l + a_4\,\,(X_{TSS})^2 + a_5\,\,(X_{TSS}\;T_l) \tag{9}$$

Values of all p_i and a_i coefficients can be found in Janus (2013, chap 7)

6. Specific cake resistance as a function of EPS content in activated sludge

Specific cake resistance under atmospheric pressure $\alpha_{c,0}$ is related to the EPS fraction in mixed liquor volatile suspended solids (MLVSS) expressed in mgTOC/gVSS using a modified expression originally proposed by Ahmed et al. (2007) and given in Eq. 10. The modification lies in introduction of a proportionality constant $m = 10$ which was added due to the fact that $\alpha_{c,0}$ values obtained from the original equation of Ahmed et al. (2007) were so small that no pressure gradients due to reversible fouling were observed in the model. TOC is calculated from COD by multiplying the COD values by a factor of three. MLVSS is calculated from MLSS using the MLVSS/MLSS ratio of 0.7.

$$\alpha_{c,0} = m\left(1.376\times10^{11}\frac{EPS}{MLVSS} - 2.564\times10^{12}\right) \tag{10}$$

7. Integrated model formulation

Structure of the integrated biological and membrane fouling MBR model (IBMF-MBR) is shown in Fig. 3 $u_i(t)$ signals represent inputs, $y_i(t)$ signals represent outputs and $w_i(t)$ denote the disturbances. The model is subdivided

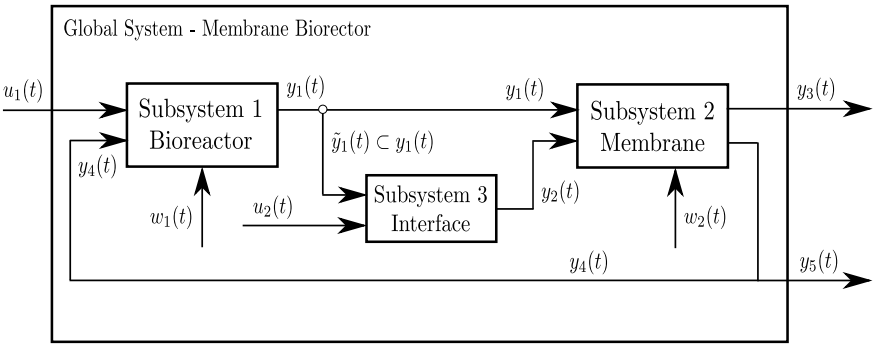

Fig. 3. Integrated MBR model structure.

into three subsystems: Bioreactor, Membrane and Interface. The Bioreactor is modelled with CES-ASM1 and the Membrane is described with Eqs. 1-7. The interface calculates specific cake resistance as a function of EPS/MLVSS according to Eq. 10, shear stresses τ_w as a function of airflow rate with the relationship obtained from the results of the slug-flow model, and oxygen transfer coefficient α as a function of MLSS with an exponential equation used in Maere et al. (2011).

The IBMF-MBR model is formulated on the plant layout defined in BSM-MBR, implemented in Simulink® and simulated with model inputs, operational parameters and simulation scenarios borrowed from the original COST Benchmark model (Copp, 2002) and BSM-MBR (Maere et al., 2011). The plant is divided into five completely stirred tank reactors (CSTRs) - two anoxic tanks, two aerobic tanks with fine-bubble aeration and one membrane tank with coarse-bubble aeration. The tank volumes are however slightly different from the ones used in BSM-MBR. In IBMF-MBR each anoxic volume is increased from $1,500$ m^3 to $1,800$ m^3 at the cost of aerobic tanks and the membrane tank whose volumes are decreased from $1,500$ m^3 to $1,300$ m^3. As a result anoxic fraction is increased from 40% to 51.4% bringing it is closer to the value recommended by MUNLV (2003) for pre-denitrification MBR plants. Anoxic fraction had to be increased because denitrification kinetics in CES-ASM1 are somehow slower from those in ASM1 due to alteration of the flow of organic substrates caused by introduction of SMP and EPS metabolic pathways.

Stoichiometric and kinetic parameters governing the SMP and EPS kinetics in CES-ASM1 are as follows: $Y_{SMP} = 0.45$, $\gamma_H = 0.0924$, $\gamma_A = 0$, $i_{XBAP} = 0.07$, $i_{XEPS} = 0.07$, $K_{UAP} = 100$, $K_{BAP} = 85$, $\mu_{UAP,20} = 0.45$, $\mu_{BAP,20} = 0.15$, $f_S = 0.4$, $f_{EPS,h} = 0.10$, $f_{EPS,dh} = 0.025$, $f_{EPS,a} = 0.0$, $f_{EPS,da} = 0.0$, $f_{BAP} = 0.0215$, $k_{h,EPS,20} = 0.17$. Description and units of all the above parameters are given in Nomenclature. Out of the original ASM1 parameters only heterotrophic biomass yield Y_H was changed from its default value of 0.67 to $0.67/(1 + 0.0924)$ gCOD gCOD^{-1}. The rest of the biological parameters were given their default values as published in Henze et al. (2000). Filtration-related parameters are as follows: $R_m = 3.0 \times 10^{12}$, $f_M = 0.5$, $b = 6.8 \times 10^{-2}$, $\Delta P_{crit} = 30,000$, $n = 0.25$, $\gamma_m = 1,500$, $\lambda_m = 2 \times 10^{-6}$. Again, description and units of all filtration-related parameters are provided in Nomenclature. The aeration model is borrowed from Maere et al. (2011) and so are all controller setpoints and operating parameters, except open-loop airflow setpoints to aeration tanks 3 & 4 which are set to 3,440 Nm^{3}h^{-1} and 3,360 Nm^{3}h^{-1}, respectively. Under closed-loop operation with DO control the airflow split ratio between tank 3 & 4 is set to 1.3 : 1. Membrane operates in a sequence of 10 min filtration periods with 1 min backwash intervals. Energy demand for aeration and mixing is calculated with the same equations as used in Maere et al. (2011). Energy demand for pumping is calculated with Equation 11 where geometric heights h_g^i, sums of hydraulic losses h_l^i and pump efficiencies η^i for each pump are provided in Table 3. The above parameters for waste flow q_w, internal recirculation q_{int} and sludge recirculation q_r were adjusted in order to match the energy costs published in Maere et al. (2011) whilst η and h_l for q_e and q_b have been assumed. Resulting geometric heights for these two flows are calculated by the membrane fouling model. Backwash flow is assumed to be twice that of the average permeate flow and corresponds to backwash flux of ~40 L m^{-2} h^{-1}.

Membrane resistance during backwash periods is assumed to be equal to $R_m + R_i$. $\rho_w = 1,000$ kg m^{-3}. t_{simu} denotes simulation time (7 days).

$$PE = \frac{60\,\rho_w\,g}{1000\,t_{simu}} \sum_{i=1}^{i=5} \frac{h_g^i + h_l^i}{\eta_i} \int_{t_0}^{t_0+t_{simu}} q_i(t)\,dt \tag{11}$$

Table 3. Parameters used in the pumping energy demand equation (Equation 11)

Parameter	Symbol	Unit	Flow				
			q_w	q_{int}	q_r	q_e	q_b
Geometric height	h_g	m	7.0	0.50	0.50	calculated	calculated
Sum of losses	h_l	m	2.17	1.42	1.42	0.5	0.5
Efficiency	η	–	0.5	0.7	0.7	0.7	0.7

IBMF-MBR is simulated in the same fashion as BSM-MBR but adopts one more control loop, i.e. nitrate control which manipulates q_{int} in order to maintain a setpoint of 1.0 mg N-NO_3^- in the second anoxic tank. The control loop design is borrowed from Copp (2002). Input files had to be modified to take into account three new variables introduced in CES-ASM1, i.e. X_{EPS}, S_{UAP}, and S_{BAP}. It is assumed that $S_{UAP} = 0$, while S_{BAP} is assumed to be equal to 70% of the influent soluble inert substrates S_I in BSM1 and BSM-MBR. X_{EPS} is assumed to constitute 5% of the biomass. EPS and BAP are assumed to contain 6% of N whilst UAP contain no nitrogen.

8. Simulation results

The simulation results show that CES-ASM1 predicts lower sludge yields and lower denitrification rates to ASM1. This behaviour is caused by the alteration of the organic substrate pathways as a result of the introduction of SMP and EPS kinetics. The results also indicate that changes in the SMP and EPS content in MLSS in response to diurnal variations in the influent flow and loading rates are too small to have a noticeable impact on membrane fouling (see Fig. 5 and Fig. 6) whilst fouling rates are highly sensitive to fluctuations of solids concentration in the membrane tank (not shown) and flux rates (Fig. 5). Such model behaviour is a direct result of the biopolymer kinetic model which does not consider biopolymer production in response to environmental stress, only due to normal variations in substrate loading. In terms of 'standard' effluent quality parameters, IBMF-MBR model predicts similar effluent TN concentrations to BSM-MBR and similar number of TN consent violations as indicated in Fig. 4, although in larger anoxic volume.

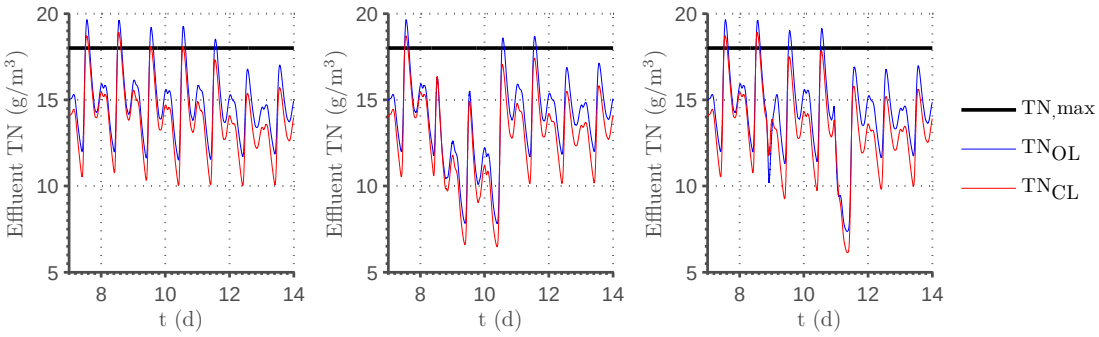

Fig. 4. Effluent total nitrogen (TN) under (a) dry- (b) rain- and (c) storm-weather and open-loop (OL) and closed-loop (CL) operation.

As shown in Table 4, IBMF-MBR in the open-loop configuration predicts similar energy demands for mixing, sludge pumping and aeration to BSM-MBR whilst in the closed-loop configuration the unit cost for membrane aeration drops significantly by 0.19 kWh m^{-3}. The energy cost for permeate pumping in IBMF-MBR is ten times less than

Table 4. Comparison of energy costs between IBMF-MBR, BSM-MBR and three municipal MBR WWTPs - modified from Maere et al. (2011)

Energy cost (kWh m^{-3})	Schilde	Varsseveld	Nordkanal	BSM-MBR	IBMF-MBR Open-loop*)	IBMF-MBR Closed-loop*)
Mixing	0.05	0.04	0.11	0.03	0.039	0.039
Sludge pumping	0.10	0.11	0.01	0.05	0.046	0.049
Effluent pumping	0.07	0.12	0.02	0.07	0.008	0.008
Aeration (bioreactor)	0.07	0.24	0.11	0.21	0.22	0.22
Aeration (membrane)	0.23	0.34	0.45	0.53	0.49	0.30
Total	0.52	0.85	0.71	0.90	0.81	0.62

*) dry-weather conditions with average permeate flow rate $q_{perm,ave}$ = 18286.3 m^3 d^{-1}

in BSM-MBR despite of rather average for an ultrafiltration (UF) module calculated permeabilities of about 80-100 Lmh bar^{-1}. On the other hand the TMP calculated in the model may not be representative for a long-term operation of a MBR due to the fact that the simulations lasted only 28 days, rather a short amount of time for slow irreversible fouling process to be taken properly into account. As a result total energy cost per m^3 of treated wastewater in BSM-MBR is, on average, 0.2 kWh m^{-3} higher than in IBMF-MBR.

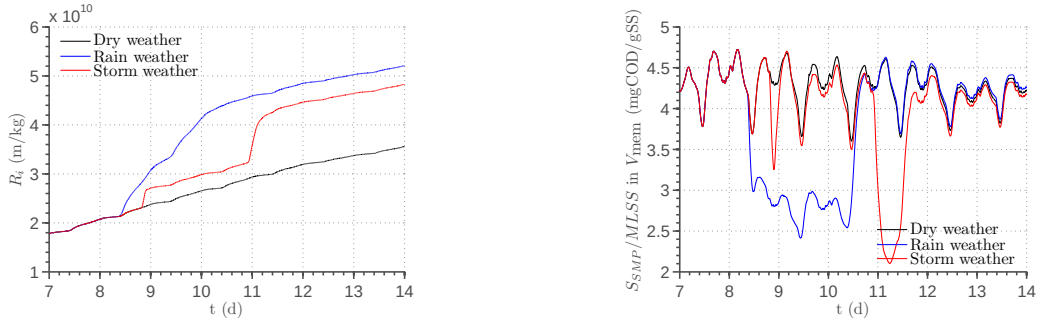

Fig. 5. (a) Irreversible fouling R_i and (b) SMP/MLSS ratio in the bioreactor during dry-, rain- and storm-events

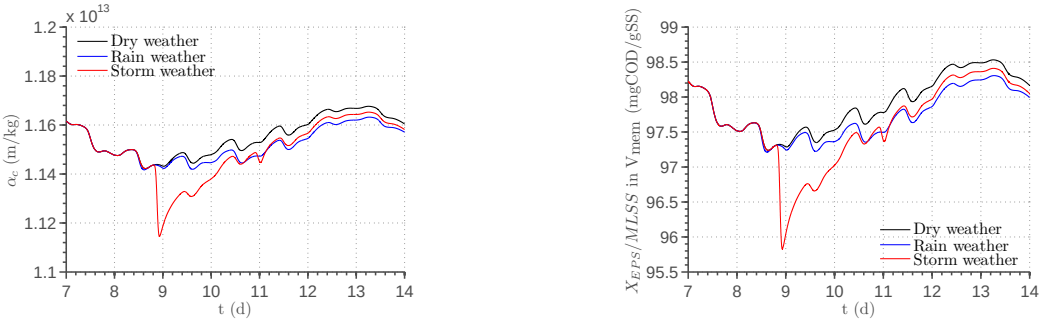

Fig. 6. (a) Specific cake resistance α_c and (b) EPS/MLSS ratio in the bioreactor during dry-, rain- and storm-events

9. Conclusions

This paper outlines the development of an integrated biological and membrane fouling MBR model (IBMF-MBR) and presents some selected simulation results. Due to space restrictions the author cannot present a full comparison of results against BSM-MBR as well as the outputs of the membrane fouling model. IBMF-MBR predicts similar effluent quality to BSM-MBR in terms of effluent ammoniacal-N, COD and TN, although the similarity in effluent TN predictions between both models had to be ascertained by increasing the anoxic volume fraction in IBMF-MBR by about 11.5% compared to BSM-MBR. The model also shows that the variations in SMP and EPS concentration due

to diurnal flow and loading patterns are not that significant to have a noticeable effect on membrane fouling which is predominantly affected by flow rate variations and fluctuations of suspended solids in the membrane tank (not shown). Whether the model is correct in predicting that the changes in biopolymer concentrations in the plant receiving diurnal flow and load patterns are so small or whether the mechanisms of biopolymer production are not sufficient to give realistic outputs, can only be ascertained through extensive validation under dynamic conditions. At the moment it seems that process setpoints such as DO, MLSS and SRT have a significantly larger influence on SMP and EPS concentrations in the bioreactor than diurnal disturbances. The last conclusion is that whilst reversible fouling can be quantified using a standard 14-day simulation benchmark time-frame, quantification of the effects of irreversible fouling requires longer simulation horizons in the range of 12 months and, possibly, a chemical cleaning model to allow simulation of irreversible fouling recovery due to periodic chemical cleaning.

References

Ahmed, Z., Cho, J., Lim, B-R., Song, K-G., Ahn, K-H., 2007. Effects of sludge retention time on membrane fouling and microbial community structure in a membrane bioreactor. Journal of Membrane Science 287, 211-218.

Aquino, S.F., Stuckey, D.C., 2008. Integrated model of the production of soluble microbial products (SMP) and extracellular polymeric substances (EPS) in anaerobic chemostats during transient conditions. Biochemical Engineering Journal 38, 138-146.

Di Bella, G., Mannina, G., Gaspare, V., 2008. An integrated model for physical-biological wastewater organic removal in a submerged membrane bioreactor: Model development and parameter estimation. Journal of Membrane Science 322, 1-12.

Böhm, L., Drews, A., Prieske, H., Bérubé, P.R., Kraume, M., 2012. The importance of fluid dynamics for MBR fouling mitigation. Bioresource Technology 122(0), 50-61.

Busch, J., Cruse, A., Marquardt, W., 2007. Modeling submerged hollow-fiber membrane filtration for wastewater treatment. Journal of Membrane Science 288(1-2), 94-111.

Copp, J.B., 2002. The COST simulation benchmark - description and simulator manual. Luxembourg: Office for Official Publications of the European Communities.

Henze, M., Gujer, W., Mino, T., van Loosdrecht, M., 2000. Activated sludge models ASM1, ASM2, ASM2d and ASM3. IWA Publishing.

Jiang, T., Myngheer, S., De Pauw, D.J.W., Spanjers, H., Nopens, I., Kennedy, M.D., Amy, G., Vanrolleghem, P.A., 2008. Modelling the production and degradation of soluble microbial products (SMP) in membrane bioreactors (MBR). Water Research 42(20), 4955-4964.

Janus, T., Paul, P., Ulanicki, B., 2009. Modelling and simulation of short and long term membrane filtration experiments. Desalination & Water Treatment 8, 37-47.

Janus, T., Ulanicki, B., 2010. Modelling SMP and EPS formation and degradation kinetics with an extended ASM3 model. Desalination 261(1-2), 117-125.

Janus, T., 2013. Modelling and Simulation of Membrane Bioreactors for Wastewater Treatment. PhD Thesis, De Montfort University, Leicester.

Laspidou, C.S., Rittmann, B.E., 2002. A unified theory for extracellular polymeric substances, soluble microbial products, and active and inert biomass. Water Research 36(11), 2711-2720.

Lee, Y., Cho, J., Seo, Y., Lee, J.W., Ahn, K-H., 2002. Modeling of submerged membrane bioreactor process for wastewater treatment. Desalination 146(1-3), 451-457.

Li, X-Y., Wang, X-M., 2006. Modelling of membrane fouling in a submerged membrane bioreactor. Journal of Membrane Science 278, 151-161.

Liang, S., Song, L., Tao, G., Kekre, K.A., Seah, H., 2006. A modeling study of fouling development in membrane bioreactors for wastewater treatment Water Environ. Res. 78(8), 857-863.

Lu, S.G., Imai, T., Ukita, M., Sekine, M., Higuchi, T., Fukagawa, M., 2001. A model for membrane bioreactor process based on the concept of formation and degradation of soluble microbial products. Water Research, 35(8), 2038-2048.

Maere, T., Verrecht, B., Moerenhout, S., Judd, S., Nopens, I., 2011. A benchmark simulation model to compare control and operational strategies for membrane bioreactors. Water Research 45(6), 2181-2190.

Mannina, G., di Bella, G., Viviani, G., 2011. An integrated model for biological and physical process simulation in membrane bioreactors (MBRs). Journal of Membrane Science 376, 56-69.

Menniti, A., Morgenroth, E., 2010. Mechanisms of SMP production in membrane bioreactors: Choosing an appropriate mathematical model structure. Water Research 44, 5240-5251.

Ministerium für Umwelt und Naturschutz, Landwirtschaft und Verbraucherschutz des Landes Nordrhein-Westfalen (Hrsg.), 2003. Waste Water Treatment with Membrane Technology (Abwasserreinigung mit Membrantechnik).

Nagaoka, H., Yamanishi, S., Miya, A., 1998. Modeling of biofouling by extracellular polymers in a membrane separation activated sludge system. Water Science & Technology 38(4-5), 497-504.

Suh, C., Lee, S., Cho, J., 2013. Investigation of the effects of membrane fouling control strategies with the integrated membrane bioreactor model. Journal of Membrane Science 429, 268-281.

Ye, Y., Chen, V., Fane, T., 2006. Modeling long-term subcritical filtration of model EPS solutions. Desalination 191(1-3), 318-327. International Congress on Membranes and Membrane Processes.

Zaisha, M., Dukler, E., 1963. Improved hydrodynamic model of two-phase slug flow in vertical tubes. Chinese Journal of Chemical Engineering 1(1), 18-29.

Zarragoitia-González, A., Schetrite, S., Alliet, M., Jáuregui-Haza, U., Albasi, C., 2008. Modelling of submerged membrane bioreactor: Conceptual study about link between activated sludge biokinetics, aeration and fouling process. Journal of Membrane Science 325, 612-624.